How to cite: *Angew. Chem. Int. Ed.* **2021**, *60*, 14030–14039
International Edition: doi.org/10.1002/anie.202102484
German Edition: doi.org/10.1002/ange.202102484

Oxygen Atom Transfer

Effect of the Ligand Backbone on the Reactivity and Mechanistic Paradigm of Non-Heme Iron(IV)-Oxo during Olefin Epoxidation

Jyoti Prasad Biswas[+], Mursaleem Ansari[+], Aniruddha Paik, Sheuli Sasmal, Sabarni Paul, Sujoy Rana, Gopalan Rajaraman,* and Debabrata Maiti**

Abstract: *The oxygen atom transfer (OAT) reactivity of the non-heme $[Fe^{IV}(2PyN2Q)(O)]^{2+}$ (**2**) containing the sterically bulky quinoline-pyridine pentadentate ligand (2PyN2Q) has been thoroughly studied with different olefins. The ferryl-oxo complex **2** shows excellent OAT reactivity during epoxidations. The steric encumbrance and electronic effect of the ligand influence the mechanistic shuttle between OAT pathway I and isomerization pathway II (during the reaction stereo pure olefins), resulting in a mixture of cis-trans epoxide products. In contrast, the sterically less hindered and electronically different $[Fe^{IV}(N4Py)(O)]^{2+}$ (**1**) provides only cis-stilbene epoxide. A Hammett study suggests the role of dominant inductive electronic along with minor resonance effect during electron transfer from olefin to **2** in the rate-limiting step. Additionally, a computational study supports the involvement of stepwise pathways during olefin epoxidation. The ferryl bend due to the bulkier ligand incorporation leads to destabilization of both d_{z^2} and $d_{x^2-y^2}$ orbitals, leading to a very small quintet–triplet gap and enhanced reactivity for **2** compared to **1**. Thus, the present study unveils the role of steric and electronic effects of the ligand towards mechanistic modification during olefin epoxidation*

Introduction

Ferryl-oxo species are the key intermediates for various natural processes such as olefin epoxidation, C–H halogenation, hydroxylation, etc.[1–7] The activity of the responsible enzymes for the transformations like oxygenases, hydroxylases, halogenases, and haloperoxidases are governed by high-valent iron-oxo intermediates.[7–9] In the synthetic scenario, several Cyt P450 model systems were utilized for olefin epoxidations and mechanistic investigations.[5,10–12] In the realm of non-heme chemistry, tetradentate ligand-based iron-complexes were employed for olefin *cis*-dihydroxylation and epoxidation reactions.[12–36] In these cases iron(V)-oxo complexes have been proposed as the active species. Non-heme manganese catalysts were also found to be suitable for asymmetric epoxidations and *cis*-dihydroxylations.[31–45]

Surprisingly the pentadentate ligand containing iron(IV)-oxo complexes are only a little explored for olefin epoxidations. A recent study has revealed that $[Fe^{IV}(N4Py)(O)]^{2+}$ can effectively transfer oxygen atom to olefins in the presence of excess triflic acid (TfOH).[46] The triflic acid coordinates with iron(IV)-oxo to facilitate the proton coupled electron transfer from olefin and subsequently favours the oxygen atom transfer to the olefin to provide the epoxides. Therefore, we opted to explore the oxygen atom transfer (OAT) reactivity of **2** with different olefins and investigate the mechanistic details (Scheme 1). In our earlier report, we have described the C–H halogenation and oxidation chemistry with sterically bulky pentacoordinate ligand (2PyN2Q) containing ferryl-oxo complex, $[Fe^{IV}(2PyN2Q)(O)]^{2+}$ (**2**).[47]

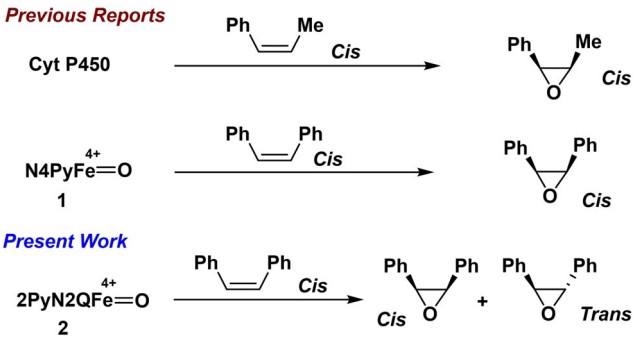

Scheme 1. Olefin epoxidation by $[Fe^{IV}(2PyN2Q)(O)]^{2+}$ (**2**), quinoline-pyridine containing ligand backbone.

Results and Discussion

Initially, we have synthesized the iron(IV)-oxo **2** by reacting iron(II)-triflate complex, $[Fe^{II}(2PyN2Q)](OTf)_2]$ (**1a**) and 1.5 equivalent of iodomesitylene diacetate in dry acetonitrile at room temperature (Figure 1). Complex **2** was spectroscopically characterized using Mossbauer, IR study, and ESI-MS measurement.[47,48] Subsequently, complex **2** was reacted with different internal and terminal olefins. The reaction of cyclooctene, norbornene with **2** provided cyclo-

[*] J. P. Biswas,[+] M. Ansari,[+] S. Sasmal, G. Rajaraman, D. Maiti
Department of Chemistry
Indian Institute of Technology Bombay
Powai, Mumbai-400076 (India)
E-mail: rajaraman@chem.iitb.ac.in
dmaiti@chem.iitb.ac.in
A. Paik, S. Paul, S. Rana
Department of Chemistry
University of North Bengal
Raja Rammohunpur, Darjeeling, West Bengal, Pin-734013 (India)
E-mail: sujoyran@gmail.com
[+] These authors contributed equally to this work.
Supporting information and the ORCID identification number(s) for the author(s) of this article can be found under: https://doi.org/10.1002/anie.202102484.

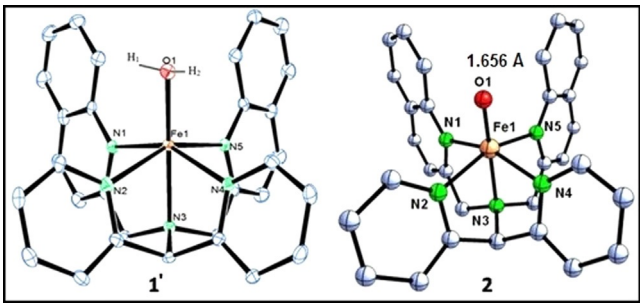

Figure 1. ORTEP diagram of aqua-coordinated iron(II)-triflate complex **1a**, $[Fe^{II}(2PyN2Q)](OTf)_2$ (CCDC: 1470119) and DFT-optimized structure of iron(IV)-oxo **2**, $[Fe^{IV}(2PyN2Q)(O)(OTf)]^{2+}$.

Table 1: Scope of epoxidation of **2** with internal olefins.[a]

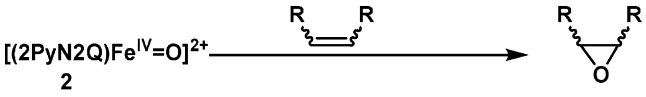

Entry	Substrate	Product(s)	
1		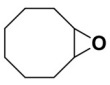	52%
2		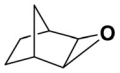	56%
3	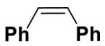	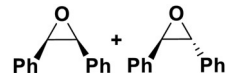	16% 36% *cis*:*trans* 1:2.2
4		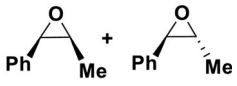	30% 14% *cis*:*trans* 1:2.2
5	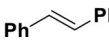	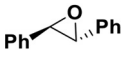	60%
6	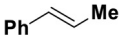	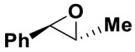	54%
7	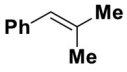	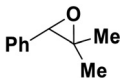	44%

[a] Reaction conditions: 2.0 mM of complex **1a** in acetonitrile, 1.5 equiv oxidant, and 100 equivalent of substrates were reacted inside the glove box.

octene oxide (52%) and norbornene oxide (56%), respectively in moderate yield (Table 1, entries 1 and 2).

Thereafter, we have tested sterically hindered *cis*-stilbene for epoxidation. Notably, *cis*-stilbene provided a mixture of *cis*-*trans* epoxides (with a ratio of *cis*:*trans* 1:2.2) with moderate yield (52%) (Table 1, entry 3). Similar *cis*-*trans* epoxide product formation was observed for *cis*-β-methyl as well (with a ratio of *cis*:*trans* 2.2:1) (Table 1, entry 4). But, both *trans*-stilbene and *trans*-β-methyl styrene provided exclusive *trans*-epoxides in moderate yields (60% and 54%, respectively) (Table 1, entries 5 and 6). Importantly, the observation of isomeric *cis*-*trans* epoxide formation from stereo pure olefins suggests that the reaction with **2** might be proceeding through a stepwise pathway. Further, terminally substituted styrene (internal olefin), 2-methyl-1-phenyl-1-propene, also provided corresponding epoxide products with good yield (Table 1, entry 7). Further, we have synthesized a soluble version of iodosobenzene that is, 1-(*tert*-butylsulfonyl)-2-iodosylbenzene, (SO_2t-Bu)PhIO[49a] and reacted 1.0 equiv of it with **1a** in acetonitrile. The resulting reaction mixture shows a UV-vis band at 770 nm, characteristic for iron(IV)-oxo species. Afterwards, we have performed the epoxidation reaction with *trans*-β-methylstyrene and obtained epoxide product albeit in low yield. Similarly, iodosylbenzene (PhIO) is solubilized in 4:1 acetonitrile-methanol and reacted with **1a**, resulting the formation of iron(IV)-oxo species (UV-vis band at 770 nm). Further, this soluble form of PhIO affords corresponding epoxide product upon reacting with *trans*-β-methylstyrene in low yield. Therefore, possibility of in situ generation of acidic species (during reaction with iodomesitylene diacetate) and its role in epoxidation reaction cannot be ruled out.[49b] Later, we have carried out the epoxidation reactions with terminal olefins. Different *para*-substituted styrene derivatives were reacted with iron-oxo **2**.

Simple styrene provided a good yield of styrene epoxide (46%) (Table 1, entry 1). Electron deficient *para*-chloro (-Cl), fluoro (-F), trifluoromethyl (-CF_3), cyano (-CN), and nitro (-NO_2) styrene derivatives also provided epoxide products in relatively less yields (Scheme 2, **2a**–**2g**). However, electron-rich *para*-methyl styrene provided *p*-methyl benzaldehyde (30%) as a major product with minor epoxide formation (20%). The product analysis during epoxidation of terminal olefins clearly indicates that electron-rich olefins (e.g. styrene) provide comparatively better yields than the electron-deficient olefins (e.g. 4-nitrostyrene). Thus, an electrophilic nature of oxidant iron(IV)-oxo complex **2** can be proposed. As the nucleophilicity of the olefins decreases, the extent of reaction (between olefin and complex **2**) as well as the yield of epoxide decreases. The modified electronic effect of weakly donating 2PyN2Q ligand compared to N4Py ligand possibly enhances the electrophilic character of complex **2**. Furthermore, we have carried out the ^{18}O labeling study during the epoxidation reactions. With the ^{18}O labeled complex **2** (prepared by addition of $H_2{}^{18}O$), when olefin substrates like *trans*-β-methyl styrene and *cis*-stilbene were

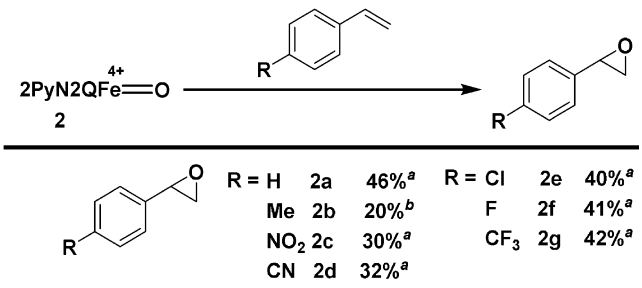

Scheme 2. Scope of epoxidation of terminal olefins by complex **2.** (2.0 mM of **1a** in acetonitrile, 1.5 equiv oxidant, and 100 equiv of substrates were reacted inside the glove box). [a] Major rearrangement product 4-methyl benzaldehyde (30%) was obtained, minor amount (< 5%) of aldehydes were obtained).

reacted, > 95 % ^{18}O labeled epoxide products were obtained in both cases (Scheme 3).[50] Thus, the labeling experiment supported that the oxygen atom of the epoxides comes from the iron(IV)-oxo complex **2**.

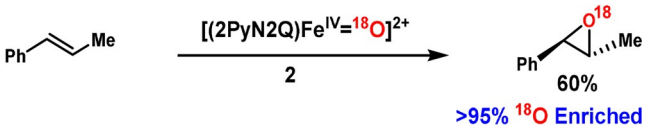

Scheme 3. Labeling experiment during olefin epoxidation by [Fe^{IV}(2PyN2Q)(O)]$^{2+}$, **2**.

Initial reactivity study with different olefins has motivated us to focus on the kinetics of olefin epoxidation to understand the mechanism of the OAT reactivity of **2** with olefins. The kinetics have been executed by monitoring the decay of the characteristic UV-vis band of **2** at 770 nm (Figure 2a,b) by

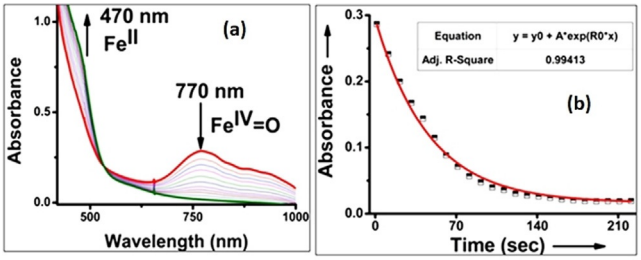

Figure 2. a) UV-vis spectra recorded during epoxidation of 4-methyl styrene by complex **2.** b) Decrease of the 770 nm band over time.

varying the concentration of the substrates under *pseudo-first-order* conditions (> 10 times stoichiometry of complex **2**) with different *para*-substituted styrene derivatives.[51–53] Subsequently, the second-order kinetics constants (k_2) were obtained from these plots. The higher values of k_2 for electron-rich styrene derivatives suggest a faster reaction rate compared to electron-deficient styrene and thus further support the electrophilic character of **2**.[54] The second-order constants (k_2's) obtained from kinetics study with styrene and its *para*-substituted derivatives have been used to construct the Hammett plot. The plot of $\log(k_X/k_H)$ against Hammett–Brown constants (σ_P^+) (considering polarity and resonance effect) shows linear correlation (Figure 3)[22] with a negative slope that is, negative reaction constant ($\rho^+ = -1$) value. Thus, it suggests the electrophilic character of iron-oxo complex **2** that possibly reacts with olefins through the transition state involving small charge separation in the rate-limiting step.[54–59] Moreover, the electron transfer from olefin (in r.d.s.) can be presumed to be governed by dominant electronic inductive effect along with minor resonance effect. Therefore, the observed reaction constant value is quite lower than some of the metal-oxo complexes and metalloenzymes mediated epoxidations reactions.[13,61–66] Further, the small negative value of the reaction constant is similar to some of the reported high-valent iron-oxo and iron(III)-acylperoxo complexes.[17,49,62] Thereafter, we have carried out kinetics of the

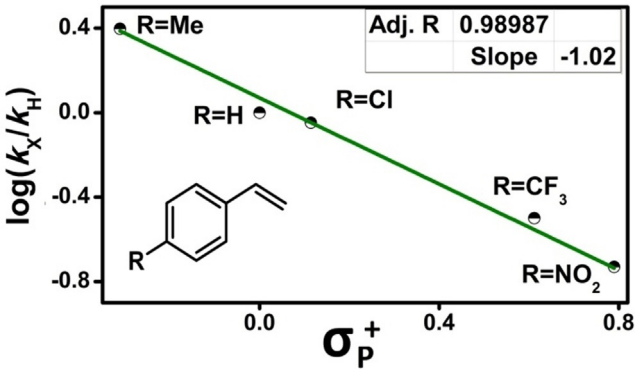

Figure 3. Hammett–Brown plot for the epoxidation of *para*-substituted styrene by complex **2**.

different internal olefins. We have studied the second-order kinetics of *cis* and *trans*-stilbene. It was found that the second-order rate constant, ($k_2 \approx 1.12\ M^{-1}S^{-1}$) of the *trans* isomer is almost ten times of the *cis*-stilbene ($k_2 \approx 0.141\ M^{-1}S^{-1}$). The higher olefin epoxidation rate of the *trans*-stilbene can be rationalized by the lower one-electron oxidation potential of the *trans*-stilbene compared to *cis*-stilbene.[67]

Evidently, we have observed major isomerization during epoxidation of pure *cis*-stilbene and *cis*-β-methyl styrene (vide supra, Table 1). Now the obvious question arises, whether the observed isomerization in the case of *cis*-stilbene *and cis*-β-methyl styrene occurs via *a* well-defined reaction pathway involving complex **2** or via a simple rearrangement between epoxide and **1**, [Fe^{II}(2PyN2Q)]$^{2+}$? In order to address this query, we have carried out the control experiment with a *cis*-stilbene epoxide in the presence of iron(II)-complex (with and without oxidant). Interestingly the control reaction does not provide any *isomerized trans* epoxide product and rules out the possibility of rearrangement reactions. Moreover, the above isomerization phenomenon suggests that epoxidation does not occur in a *concerted pathway*; instead, it might proceed in a *stepwise pathway* upon reaction with **2** involving a neutral radical intermediate.[68]

Thus, in the present study a longer lifetime of intermediate **IM**$_{cis}$ is expected so that C-C rotation becomes feasible to provide isomerized product (Scheme 4).[54,58,69] The present observation of *isomerization* in the stepwise mechanism is in contrast with Cyt-P450 enzymes mediated epoxidations. Interestingly, after the formation of intermediate **IM**$_{cis}$, there are two possible pathways by which it can react: firstly, if *pathway I* occur preferentially over *pathway II* then the only *cis*-epoxide product is expected (Scheme 4). Secondly, if there is a competition between these two pathways (I and II) then a mixture of *cis* and *trans* epoxide should be obtained. Clearly, our findings are consistent with the second possibility, that is, after the stepwise formation of *intermediate I*, the competition between *pathway I* and *II* results in a mixture of epoxides (Scheme 4). In contrast with the above phenomenon, the pentadentate pyridine-pyridine ligand (N4Py) containing iron(IV)-oxo, **1** with *cis*-stilbene and provides only *cis*-stilbene epoxide. Possibly, the presence of quinoline moiety in the 2PyN2Q ligand creates enough steric bulk that triggers the mechanistic shuttle between *pathway II* and *pathway I*.

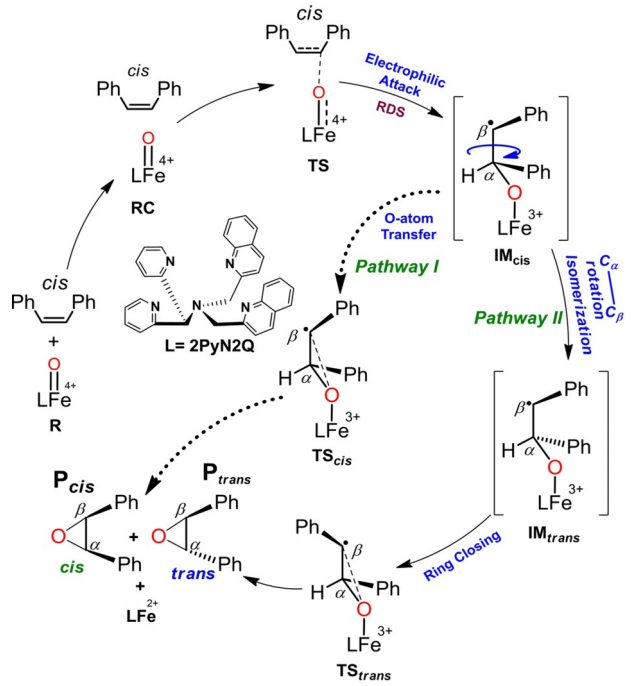

Scheme 4. Schematic mechanism for the formation of a *cis* and *trans* epoxide from complex **2**.

Also, the extent of isomerization (*cis*:*trans* epoxides products) between *cis*-stilbene and *cis*-β-methyl styrene (Table 1) clearly shows the dependency of the extent of *isomerization* pathway (*pathway II*) on the steric bulk of both ligand and reactants. Additionally, the detailed computational study is performed to unravel the mechanistic intricacies in depth, is discussed in the following section.

Theoretical Study

Based on earlier reported experimental and theoretical studies, we have proposed a mechanism for the conversion of an alkene to epoxide. DFT calculations (B3LYP-D2/6-31G(LanL2DZ-Fe)//B3LYP-D2/TZVP setup[48,70–72]) have been performed on the formation of $Fe^{III/IV}$-oxo species, which is used for the catalysis (also see ESI for the additional writeup on the formation of the $Fe^{III/IV}$=O species). For understanding the reaction mechanism, we have started our calculations on the active catalyst $[(2PyN2Q)Fe^{IV}=O]^{2+}$ (**2**) species. The computed energetics reveal that the triplet state (^{3}**2**$_{(is)}$) is the ground state with ^{5}**2**$_{(hs)}$, and ^{1}**2**$_{(ls)}$ states lying at 3.8 and 122.4 kJ mol^{-1}, respectively. Computed energetics, the nature of the ground state, and the structural features are consistent with previously reported experimental and theoretical data.[71,73–75] For ^{3}**2**$_{(is)}$ spin state, Fe^{IV}=O, Fe^{IV}-N_{py}, Fe^{IV}-N_Q, and Fe^{IV}-N_{amine} bond lengths are computed to be 1.656 Å, 1.999 Å, 2.047 Å, and 2.057 Å, respectively. The X-ray structure of **2** is reported where Fe^{IV}=O, Fe^{IV}-N_{py}, Fe^{IV}-N_Q, and Fe^{IV}-N_{amine} bond lengths are found to be 1.677 Å, 2.022 Å, 2.067 Å, and 2.084 Å, respectively. These values are consistent with the computed structure. Computed bond lengths show that Fe-N_{py} distances are slightly shorter than the Fe-N_Q distances (Figure 4a). A bond angle (N-Fe-O) of 171.4° was observed corresponding to the ferryl oxygen atom.[48,76] This ferryl-bend is also consistent with the X-ray structure of **2** (170.5°).[48] Interestingly, unlike most of the Fe^{IV}=O species, which are found to be linear, the bond angle N-Fe-O is found to be bend towards the pyridine ring owing to the presence of a bulkier quinoline group. In species **2**, we observed two strong C–H···O interactions between the C–H atom of the quinoline and ferryl-oxygen atom, consequently the distances were noted to be 2.021 Å, which is also in accord with experiments. These interactions and ferryl-bending are expected to increase the reactivity of this species compared to $[(N4Py)Fe^{IV}=O]^{2+}$ species.[50,77–79] Our computed spin density value for the ground state (^{3}**2**$_{(is)}$) on Fe and O atom is noted as 1.04 and 0.98 (see Figure S29a and S30–S32 in ESI). Both triplet and quintet state exhibit strong ferryl bending, and this leads to significant polarization of the spin density. Compared to $[(N4Py)Fe^{IV}=O]^{2+}$ species, in **2** the equatorial donations are much weaker, leading to a very small triplet-quintet gap suggesting the possibility of two-state reactivity.[80–82] Natural Bond Orbital (NBO) analysis was performed on species **2** at the B3LYP/TZVP level, which explains the nature of bonding, intramolecular rehybridization, and delocalization of electron density within the molecule (see Figures S33 and S34 in ESI).

The computed Fe-O vibrational stretching is found to be 819 cm^{-1}. This value is slightly underestimated compared to the experimental value of 834 cm^{-1} reported for the species **2**.[48] Both experimental and theoretical Fe-O vibrational stretching are found to be lower than the value reported for known Fe^{IV}=O bond, and this is essentially due to the ferryl-bend in combination with two weak CH···O interactions present in species **2**. The computed quadrupole splitting and isomer shift values are 0.51 and 0.02 mm s^{-1}, respectively, and these are in agreement with the experimental estimates of 0.56 and 0.03 mm s^{-1}, respectively. The computed zero-field splitting parameter (D) value is 25.4 cm^{-1}, and this is close to the experimental estimate of 24.3 cm^{-1}. The calculated structural parameters offer confidence in our methodology used for calculations.[47]

Epoxidation of cis*-Stilbene by 2 (R)*

Based on the experimental inputs, the mechanism shown schematically in Scheme 4 is adapted for our calculations.[66,83,84] Indeed, there is a growing recognition that the reactions of Fe^{IV}=O unit with olefins undergo in a stepwise manner.[73] In the stepwise mechanism, the olefin approaches the Fe^{IV}=O (**R**) centre in an end-on fashion to form a reactant complex (**RC**). After the formation of **RC**, an electrophilic attack of the Fe^{IV}=O unit on the carbon atom of the alkene via transition state (**TS**) takes place, followed by the formation of the O–C bond leading to Fe^{III}-radical intermediate $\mathbf{IM}_{cis}$.[83,84] This radical intermediate can undergo either O–C bond formation via $\mathbf{TS}_{cis}$, to the form *cis*-epoxide or C–C rotation, leading to *trans* radical intermediate $\mathbf{IM}_{trans}$, which further undergoes O–C bond formation via $\mathbf{TS}_{trans}$, leading to the *trans*-epoxide formation (Scheme 4).

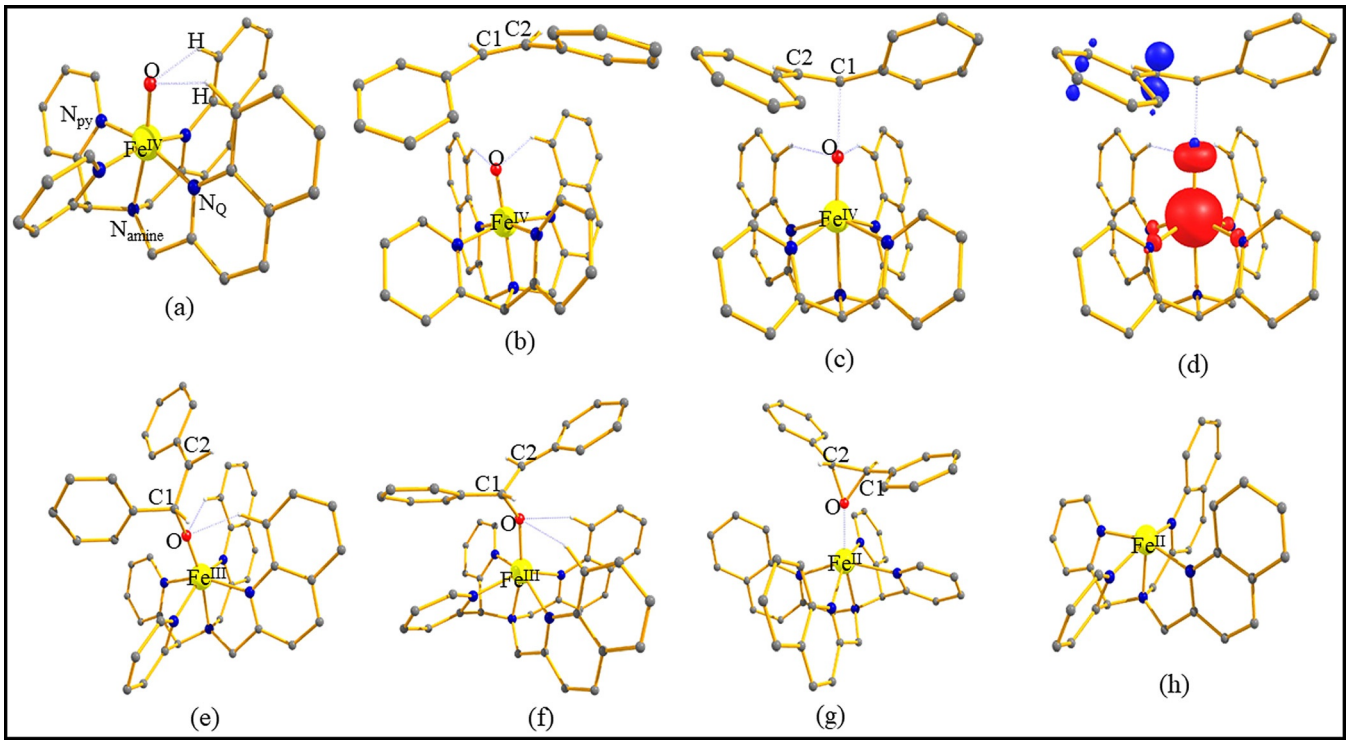

Figure 4. Optimized structures of a) ^{3}**2**$_{(is)}$, b) ^{3}**RC**$_{(is)}$, c) ^{5}**TS**$_{(hs)}$ along with d) the corresponding spin density plot, e) ^{5}**IM1c**$_{is(hs)}$, f) ^{5}**TS**$_{trans(hs)}$, g) ^{5}**IM2t**$_{rans(hs)}$, and h) ^{5}**P**$_{(hs)}$. Some important structural parameters computed for the spin states and spin density values are given below for species **2** (**R**), **RC**, **TS**, **IM1c**$_{is}$, ^{5}**TS**$_{trans(hs)}$, ^{5}**IM2t**$_{rans(hs)}$ and ^{5}**P**$_{(hs)}$. For spin state ^{3}**2**$_{(is)}$: Fe^{IV}-O = 1.656, Fe^{IV}-N$_{py}$ = 1.999, Fe^{IV}-N$_Q$ = 2.047, Fe^{IV}-N$_{amine}$ = 2.057, Fe^{IV}-N$_{avg}$ = 2.029 and C–H···O = 2.021, ∠N$_{amine}$-Fe^{IV}-O = 171° and ∠N$_{eq}$-Fe^{IV}-O = 93°. For spin state ^{3}**RC**$_{(is)}$: Fe^{IV}-O = 1.655, Fe^{IV}-N$_{py}$ = 1.994, Fe^{IV}-N$_Q$ = 2.053, Fe^{IV}-N$_{amine}$ = 2.058, Fe^{IV}-N$_{avg}$ = 2.029, O-C1 = 3.583, O-C2 = 3.944 and C–H···O = 2.018, ∠N$_{amine}$-Fe^{IV}-O = 172°, ∠N$_{eq}$-Fe^{IV}-O = 93°, ∠Fe^{IV}-O-C1 = 155° and ∠Fe^{IV}-O-C2 = 145°. For spin state ^{5}**TS**$_{(hs)}$: Fe^{IV}-O = 1.746, Fe^{IV}-N$_{py}$ = 2.227, Fe^{IV}-N$_Q$ = 2.243, Fe^{IV}-N$_{amine}$ = 2.283, Fe^{IV}-N$_{avg}$ = 2.238, O-C1 = 2.229, O-C2 = 2.719 and C–H···O = 2.189, ∠N$_{amine}$-Fe^{IV}-O = 171°, ∠N$_{eq}$-Fe^{IV}-O = 97°, ∠Fe^{IV}-O-C1 = 174°, ∠Fe^{IV}-O-C2 = 149° and ∠C1-O-C2 = 31° and spin density Fe^{IV} = 3.81, O = 0.50, C1 = −0.06, C2 = −0.39 and C atoms of benzene = −0.05. For spin state ^{5}**IM1c**$_{is(hs)}$: Fe^{III}-O = 1.800, Fe^{III}-N$_{py}$ = 2.208, Fe^{III}-N$_Q$ = 2.234, Fe^{III}-N$_{amine}$ = 2.251, Fe^{III}-N$_{avg}$ = 2.228, O-C1 = 1.487, O-C2 = 2.460 and C–H···O = 2.371, ∠N$_{amine}$-Fe^{III}-O = 170°, ∠N$_{eq}$-Fe^{III}-O = 96°, ∠Fe^{III}-O-C1 = 179°, ∠Fe^{III}-O-C2 = 145° and ∠C1-O-C2 = 110°. For spin state ^{5}**TS**$_{trans(hs)}$: Fe^{III}-O = 2.017, Fe^{III}-N$_{py}$ = 2.150, Fe^{III}-N$_Q$ = 2.165, Fe^{III}-N$_{amine}$ = 2.233, Fe^{III}-N$_{avg}$ = 2.173, O-C1 = 1.562, O-C2 = 1.731 and C–H···O = 2.351, ∠N$_{amine}$-Fe^{III}-O = 163°, ∠N$_{eq}$-Fe^{III}-O = 93°, ∠Fe^{III}-O-C1 = 169° and ∠Fe^{III}-O-C2 = 138°. For spin state ^{5}**IM2t**$_{rans(hs)}$: Fe^{II}-O = 2.147, Fe^{II}-N$_{py}$ = 2.253, Fe^{II}-N$_Q$ = 2.262, Fe^{II}-N$_{amine}$ = 2.243, Fe^{II}-N$_{avg}$ = 2.255, O-C1 = 1.564, O-C2 = 1.561 and C–H···O = 2.466, ∠N$_{amine}$-Fe^{II}-O = 167°, ∠N$_{eq}$-Fe^{II}-O = 92°, ∠Fe^{II}-O-C1 = 159° and ∠Fe^{II}-O-C2 = 142°. For spin state ^{5}**P**$_{(hs)}$: Fe^{II}-N$_{py}$ = 2.203, Fe^{II}-N$_Q$ = 2.134, Fe^{II}-N$_{amine}$ = 2.149 and Fe^{II}-N$_{avg}$ = 2.165. All bond lengths are given in Å and angles are given in °. All hydrogen atoms (except H-C(1) = C(2)-H and C–H···O are omitted for clarity.

Here, three possible spin states have been computed, and triplet ^{3}**RC**$_{(is)}$ is found to be the ground state while other spin states are high lying in energy at 13.9 and 125.2 kJ mol^{-1}, for quintet and singlet states, respectively. The computed ground state energy for the reactant complex (^{3}**RC**$_{(is)}$) is estimated to be 56.1 kJ mol^{-1} from ^{3}**R**$_{(is)}$ (Figure 5). Computed bond lengths for ground state in the Fe^{IV}=O, Fe^{IV}-N$_{avg}$, O-C1, and O-C2 are 1.671 Å, 2.131 Å, 3.230 Å, and 3.402 Å (Figure 4b), respectively. We have also computed spin density values on Fe^{IV}, O, C1, and C2 for the ground state, and the values came out to be 1.03, 0.99, 0.01, and 0.00, respectively (see Figure S29b in ESI). In the reactant complex (**RC**), both the ^{3}**RC**$_{(is)}$ and the ^{5}**RC**$_{(hs)}$ states are energetically accessible, suggesting a possibility of two-state reactivity (Figure 5). For the transition state (**TS**), all three possible spin states have been computed, ^{5}**TS**$_{(hs)}$, ^{3}**TS**$_{(is)}$, and ^{1}**TS**$_{(ls)}$. The ^{5}**TS**$_{(hs)}$ is found to be the ground state, and with the calculated barrier height of 146.5 kJ mol^{-1} (Figure 5) for C=C bond activation of *cis*-stilbene in case of the ^{3}**TS**$_{(is)}$. However, this is not the lowest energy pathway as the ^{5}**TS**$_{(hs)}$ transition state is found to have a barrier height of 88.5 kJ mol^{-1} from the ^{3}**R**$_{(is)}$ surface. This certainly demands a minimum energy crossing point (MECP)[85] between the two spin surfaces, the spin-orbit coupling and large anisotropy are estimated for these states. A facile spin crossover is expected.[85] Although different substrates are used, our computed barrier heights are consistent with earlier reported values for the epoxidation by different Fe^{IV}=O complexes.[85–87] With respect to the reactant Fe–O, as well as the C=C bonds were elongated. Partial delocalization of the spin densities on the iron and oxygen atoms to the adjacent olefinic carbon atom was found. In the transition state, Fe^{IV}=O bond length elongates to 1.746 Å, compared to the bond length in the reactant (1.656 Å), and simultaneously, the Fe^{IV}–N$_{avg}$ bond length also elongates. The length of the newly forming O···C1 bond in the transition state was computed to be 2.229 Å (Figure 4c), and

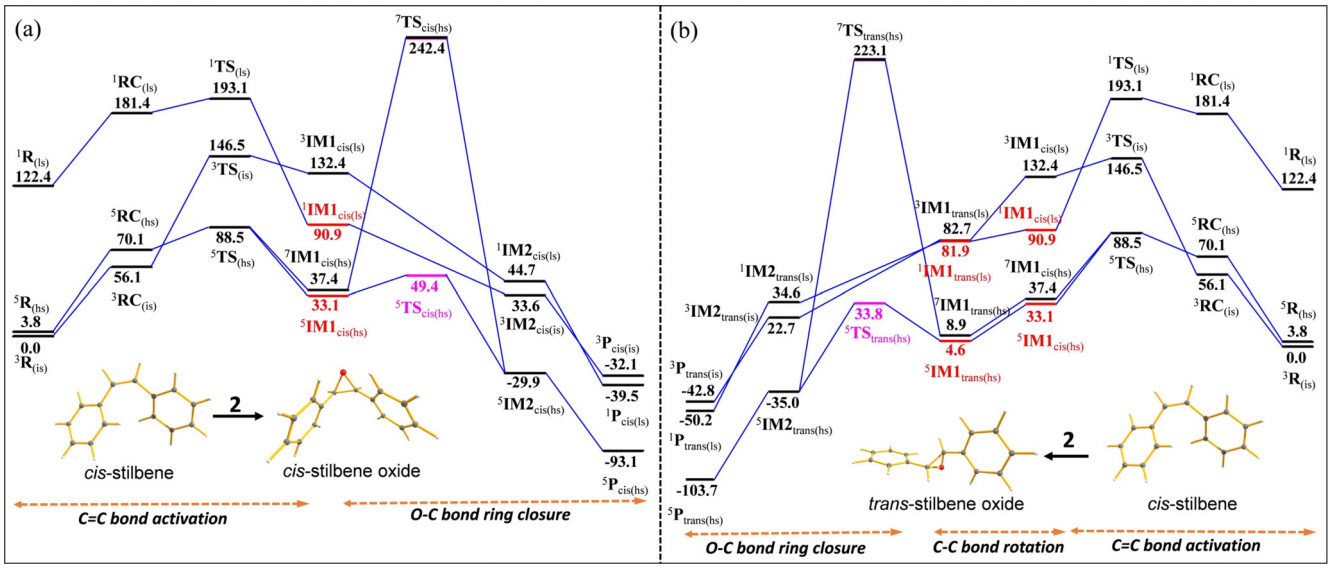

Figure 5. B3LYP-D2 computed energy profile diagram for C=C bond activation of *cis*-2-stilbene by species $[Fe^{IV}(2PyN2Q)=O]^{2+}$: a) *cis*-epoxidation and b) *trans*-epoxidation pathways (energies are given in kJ mol^{-1}). The red vertical line represents single point calculations performed on the corresponding ferromagnetic state, while the magenta vertical line represents barrier heights estimated from a relaxed scan performed for the corresponding coordinate (see S36 and S37 in ESI).

the C1···C2 bond is nearly a single bond (1.404 Å). The computed energy profile diagram is illustrated in Figure 5. In the transition state, the O···C1 bond formation spurs the generation of a radical character on the carbon atom (C2), suggesting a radical type intermediate and not cationic or anionic intermediate. Computed optimized geometries and spin density plots for ground spin state obtained are shown in Figure 4c, d. The spin density value on the Fe^{IV} of ^{5}**TS**$_{(hs)}$ state is noted as 3.81, and for O atom, C1, C2 atoms of the benzene ring are noted as 0.50, −0.06, −0.39, and −0.05, respectively, with small overall charge (group charge $Q_{C2}=0.03$ and Figure 4d). Spin density values indicate that the one α-electron transfer from *cis*-stilbene to the Fe^{IV} centre, but β-electron remains present on the carbon centre (C2) of the *cis*-stilbene (Figure S35 and S36 in ESI). Spin density values also suggest that the radical intermediate is formed during the course of the reaction and is corroborated with experimental data. The orbital evolution diagram[85,88] and Eigen-value plot are shown in Figures S35 and S36. This emphasizes the species emerging from the doubly degenerate ground state, ^{3}**R**$_{(is)}$, during C−C epoxidation. During C=C bond activation, an electron shifts from $\pi_{C\text{-}C}$ orbital of olefin to one of the d-based orbitals in ^{5}**R**$_{(hs)}$, leading to six different spin states for the *cis* intermediates. A ferryl oxygen atom attack on the C=C bond leads to the formation of a radical intermediate that is found to be delocalized on the benzylic carbon atoms. The *cis* radical intermediate is converted into *trans* intermediate by rotation of the C-C bond leading to a mixture of products. As expected, an elongation of the Fe−O bond occurs along with O-C1 bond closures, and the (**IM1**$_{cis/trans}$). Among six possible spin states, ^{7}**IM1**$_{cis/trans(hs)}$ and ^{3}**IM1**$_{cis/trans(ls)}$ intermediates were successfully optimized, and the energies of antiferromagnetically coupled state between the Fe^{III} and carbon radical centre were obtained by performing single point (SP) calculations from the corresponding ferromagnetic state. Here, the ^{5}**IM1**$_{cis(hs)}$ and ^{5}**IM1**$_{trans(hs)}$ are found to be the ground state, while other intermediate species are higher in energy (Figure 5). For ^{5}**IM1**$_{cis/trans(hs)}$ spin state, Fe^{III}-O, Fe^{III}-N_{avg}, O-C1, and O-C2 bond lengths are computed to be 1.800/1.805 Å, 2.228/2.222 Å, 1.487/1.491 Å, and 2.461/2.448 Å, respectively (Figure 4e). Computed spin density values for $^{5/7}$**IM1**$_{cis/trans(hs)}$ state on Fe^{III}, O, C1, C2, and benzene ring are noted as 3.95/3.93, 0.45/0.43, 0.06/0.06, −0.65/−0.59, and −0.22/−0.20 (see Figure S29c in ESI). The spin density values clearly suggest that the β-electron is delocalized over the benzene as well as present on the carbon centre (C2), which is connected to the carbon centre (C1) (see Figure S29c in ESI).

In the ring-closing steps, the O-C2 bond elongates to make a bond at the same time the Fe^{III}−O bond is also elongated. The ^{5}**TS**$_{cis/trans(hs)}$ is found to be the ground state, while other spin states are high in energy (Figure 5). The computed bond lengths for Fe^{III}-O and O-C2 of ^{5}**TS**$_{cis/trans(hs)}$ are 2.015/2.018 and 1.739/1.731 Å, respectively (Figure 4f). The computed spin density for the ^{5}**TS**$_{cis/trans(hs)}$ on the Fe^{III}, O, and C2 are 3.71/3.71, 0.02/0.03, and 0.03/0.02, respectively (see Figure S39a in ESI). The product selectivity is decided by the transition state of O-C2 bond formation, and this recombination of the O-C2 bond is found to be 33.9 kJ mol^{-1} for *trans* product and 49.4 kJ mol^{-1} for a *cis* product from the reactant. The energy difference between ^{5}**TS**$_{trans(hs)}$ and ^{5}**TS**$_{cis(hs)}$ is estimated to be 15.6 kJ mol^{-1}, and energetic data also suggest that the trans epoxide is expected to be the dominant product, as revealed in the experiments. When we compared the barrier heights of C=C bond activation with the O-C rebound step, the former is substantially larger and hence is the rate-determining step.

In the consequent step, the O−C bond formation leads to the generation of Fe^{II}-epoxide adduct (**IM2**). We have

calculated all possible spin states ^{5}**IM2**$_{cis/trans(hs)}$, ^{3}**IM2**$_{cis/trans(is)}$, and ^{1}**IM2**$_{cis/trans(ls)}$. The ^{5}**IM2**$_{cis/trans(hs)}$ is found to be the ground state, while other spin states are high in energy (Figure 5). The bond lengths for Fe-O of ^{5}**IM2**$_{cis/trans(hs)}$ are 2.178/2.147 Å (see Figure 4g and S39b in ESI). The *trans* Fe^{II}-epoxide adduct is found to be more stable than the *cis* adduct (Figure 5). The energy difference between *trans* and *cis* intermediate is estimated to be 5.1 kJ mol^{-1}.

In the last step, the Fe–O bond cleaves from the Fe^{II}-epoxide adduct leading to the generation of the final product with the overall thermodynamic stabilization of −103.7 kJ mol^{-1} (Figure 5, Figure 4h and S39c in ESI). ^{5}**P**$_{trans(hs)}$ isomer is thermodynamically more stable than the ^{5}**P**$_{cis(hs)}$ by 10.7 kJ mol^{-1}. All the energetics computed reveal that a racemic mixture of *trans*- and *cis*-product is expected as observed in experiments. We have also calculated the ratio of the product formation using the ring-closing transition state energy barrier. The ratio of product formation is found to be 1:2.2 for *cis*:*trans* isomer, which is consistent with experimental data. The single turnover epoxidation of *cis*-stilbene using species **2** yields a mixture of 16% *cis* and 36% *trans*-stilbene oxides, revealing that the *trans*- epoxide is dominant over *cis*-epoxide product. Due to this reason, we have also performed calculations on the *trans*- stilbene using **2**, and calculated barrier height on the quintet surface of this reaction is found to be 83.2 kJ mol^{-1} from the reactant (^{3}**R**$_{(is)}$). The computed barrier height suggested that the formation of *trans*-epoxide (60%) product is more preferred than the *cis*-epoxide product, which is also corroborated with the experimental data (Table 1, entry 5 and see Figure S40 in ESI).

While the epoxidation and the racemization of the stereochemistry are understood, we turn to understand the electronic origin behind the reactivity of $[(2PyN2Q)Fe^{IV}{=}O]^{2+}$ (**2**) compared to $[(N4Py)Fe^{IV}{=}O]^{2+}$ (**1**) species,[89] which does not perform epoxidation without additives. We have chosen *cis*- stilbene as a substrate computed the energetics associated with the epoxidation reaction for species **2**. Firstly, we have observed that both complexes have an intermediate spin state ($S=1$) as a ground state. But, our calculations suggest that the quintet-triplet gap is very small (3.8 kJ mol^{-1}) in the case of species **2**, while the quintet-triplet gap is relatively large (19.6 kJ mol^{-1}) for species **1**.[90] The quintet-triplet gap is higher for species **1** due to the presence of strong nitrogen atoms donation at the equatorial as well as axial positions compared to species **2**, as affirmed by Fe–N bond lengths for the former (Fe^{IV}-N_{avg} = 2.029 Å for species **1**, and Fe^{IV}-N_{avg} = 2.000 Å for species **2**).[14,90] Two different donor nitrogen atoms present in the equatorial position accompanied by the ferryl bend wherein N-Fe=O angle in species **2** leads to stabilization of the corresponding d_{z^2} and $d_{x^2-y^2}$ orbitals compared to the species **1** (see Figure S41 in ESI).[47,48,90] This leads to the smaller quintet-triplet gap. In fact, the gap in **2** is so small that a mean-energy crossing point from the triplet to quintet is not required for the reactivity, while for species **1**, this is mandatory suggesting additional energy penalties which tend to slow down the reaction. We have also computed the Natural Population Analysis (NPA) charges for both complexes, which suggest species **2** to be more electrophilic than **1** (Fe; O charges are 0.35; −0.28 and 0.28; −0.25 for the former and the latter, respectively).

The potential energy surface constructed for species **1** promoting epoxidation of *cis*-stilbene is shown in Figure 6 (see Figure S42 in ESI for optimized structures and spin density plots of ground state). Clearly, the reactivity here as well originates from the quintet state with the estimated barrier height of 97.7 kJ mol^{-1}, which is 9.1 kJ mol^{-1} higher compared to the same for species **2**.

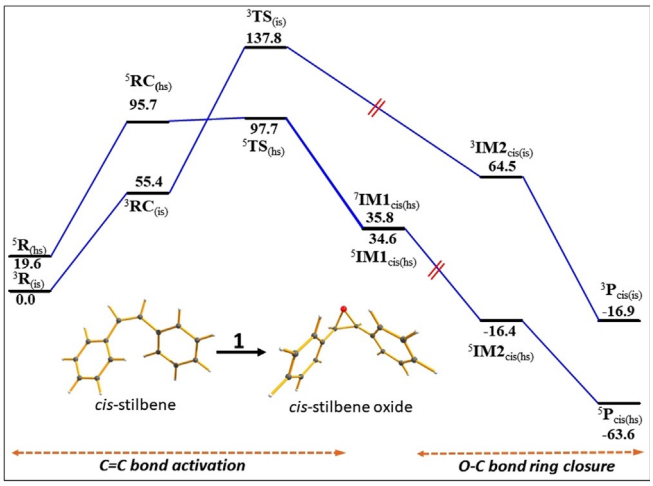

Figure 6. B3LYP-D2 computed energy profile diagram for C=C bond activation of *cis*-2-stilbene by $[(N4Py)Fe^{IV}{=}O]^{2+}$ (**1**) species (energies are given in kJ mol^{-1}).

To underpin the origin of this difference in the barrier, we have looked at carefully the HOMO–LUMO gap between the substrate and the catalyst.[91] For species **2**, the energy difference between the LUMO of the Fe=O σ^* and C=C orbital of *cis*-stilbene is 1.06 eV at the quintet surface, while for species **1** is found to be 1.19 eV at the same spin surface. These HOMO–LUMO gaps are suggesting that species **2** is more reactive towards C=C activation of *cis*-stilbene than species **2**. Interestingly, we have found comparable dipole moment values for 6.86 D of species **2** and 4.70 D for **1**. These dipole moment values are also suggesting that the species **2** is more reactive towards C=C activation of *cis*-stilbene than species **1**.

Additionally, we have also performed an energy decomposition analysis (EDA) for **1** and **2** by treating N4Py/2PyN2Q, Fe, and O as separate fragments ({N4Py}/{2PyN2Q} + {Fe} + {O}) (see Table 5 in ESI). The calculated EDA results for **1** and **2** are found to be −4180.1 and −3930.8 kJ mol^{-1}, respectively, which shows that the ΔE_{int} for $[(2PyN2Q)Fe^{IV}{=}O]$ is smaller than the $[(N4Py)Fe^{IV}{=}O]$. These ΔE_{int} values are suggesting that species **2** is less stable than species **1** and account for the fact that **2** is more reactive towards C=C bond activation than **1**. A significant contribution to the interaction energy for **1** arises from orbital stabilization, indicating a stronger metal-ligand (Fe-L) bond for **1** compared to **2**. NBO second-order perturbation analysis reveals a significant difference present in the σ-bonding interactions between these two species. The σ-bonding

interaction is found to be composed of Fe(d_{z^2})-O(p_z) orbitals, and the stabilization energies for **2** is 151.8 kJ mol^{-1}, which is smaller compared to species **1** (161.9 kJ mol^{-1}). Besides, the Fe–O bond in species **2** is found to be less covalent in nature compared to the Fe–O bond in species **1** (37.03 % Fe (d_{z^2}) and 62.97 % of O(p_z) for **1** and 35.06 % Fe(d_{z^2}) and 64.94 % of O(p_z) for **2**) (see Figure S41 and S42 in ESI).

Additionally, the {(N4Py)Fe^{II}-epoxide} product is also found to be not as stable as the one corresponding to [(2PyN2Q)Fe^{II}-epoxide] species. The cleavage of the epoxide from the {Fe^{II}-epoxide} product was found to be less exothermic for N4Py ligand architecture compared to 2PyN2Q ligand architecture (−46.9 kJ mol^{-1} vs. −68.7 kJ mol^{-1} for N4Py and 2PyN2Q, respectively). This is essentially due to the shorter Fe-O(epoxide) distance found for the N4Py suggesting a product inhibition in action, even if epoxide formation results.[14,85]

Further, we have also probed the origin of a large difference in the barrier height of the quintet transition state between two-ligand architecture by calculating the deformation energies. Calculations reveal that while steric factor contributes nearly 68.8 ± 1.6 % to the barrier height for both the ligands, the interaction energy between the fragments found to add a significant penalty for the N4Py compared to 2PyN2Q ligand architecture (29.6 kJ mol^{-1} vs. 28.6 kJ mol^{-1} for N4Py and 2PyN2Q, respectively). Thus, lesser steric repulsion and less favourable orbital stabilization are the main reason for N4Py to be unreactive towards olefin under normal reaction conditions. All these collectively lead to extremely slow or no reactivity at all for the N4Py ligand architecture, while the addition of two quinolines was found to promote a significant change with respect to steric and electronic behaviour. A similar correlation on the epoxidation of olefin is also observed earlier in different ligand architecture.[14,73,85]

Conclusion

In summary, quinoline-pyridine ligand (2PyN2Q) containing ferryl-oxo complex **2** has successfully performed epoxidation of different internal and terminal olefins. The electronic environment and steric bulk from 2PyN2Q ligand in **2** facilitate epoxidation and mechanistic shuttle between *oxygen atom transfer pathway* and *C=C rotation pathway* from the intermediate (**IM**$_{cis}$). Thus, the present study unveils the role of electronic and steric effects on iron(IV)-oxo complex from the ligand backbone on the reactivity of olefin epoxidation. DFT study was performed to investigate the nature of the oxidant in non-heme iron catalytic systems and its mechanism of formation. Calculations reveal that the activation of olefin by the Fe^{IV}=O is found to be rate-limiting, with the radical species gaining stability and lifetime. This allows easy C–C bond rotation leading to thermodynamically more stable *trans* radical intermediate, which yields *trans*-epoxide with facile ring closure step leading to the enhanced *trans* product compared to *cis*-epoxide. All the mechanistic findings are consistent with the experiments. Further, our calculations performed on [(N4Py)Fe^{IV}=O]$^{2+}$ species reveal some key differences, however minor, lead to a dramatic difference in the reactivity between the two species. This comparative study has interesting implications in biomimetic/enzymatic chemistry. Various amino acid residues coordinate to Fe could play a role in fine-tuning the reactivity by inducing a "ferryl" bend also could alter the electronic structure and enhance the reactivity. This aspect has not been fully explored yet in both heme, and non-heme Fe^{IV}=O catalyzed enzymatic reactions.

Acknowledgements

This activity is supported by SERB, India (CRG/2018/003915). G.R. would like to thank CSIR and SERB (01(2980)/19/EMR-II, CRG/2018/000430; DST/SJF/CSA-03/2018-10; SB/SJF/2019-20/12) New Delhi, for financial support. S.R. acknowledges SERB for Start-Up Grant (SRG/2019/000310). Financial support has been received from CSIR-India (fellowship to J.P.B. and S.S.). M.A. would like to thank IITB for funding. A.P. acknowledges SERB for the Project Assistant Fellowship in Start-Up Grant (SRG/2019/000310).

Conflict of interest

The authors declare no conflict of interest.

Keywords: biomimetic synthesis · epoxidation · ligand effects · non-heme iron-oxo · oxygen atom transfer

[1] J. Jasniewski, L. Que, *Chem. Rev.* **2018**, *118*, 2554 – 2592.
[2] S. Sahu, D. P. Goldberg, *J. Am. Chem. Soc.* **2016**, *138*, 11410 – 11428.
[3] M. Guo, T. Corona, K. Ray, W. Nam, *ACS Cent. Sci.* **2019**, *5*, 13 – 28.
[4] M. Sankaralingam, Y.-M. Lee, W. Nam, S. Fukuzumi, *Coord. Chem. Rev.* **2018**, *365*, 41 – 59.
[5] X. Huang, J. T. Groves, *J. Biol. Inorg. Chem.* **2017**, *22*, 185 – 207.
[6] J. P. Biswas, S. Guin, D. Maiti, *Coord. Chem. Rev.* **2020**, *408*, 213174.
[7] S. Rana, J. P. Biswas, S. Paul, A. Paik, D. Maiti, *Chem. Soc. Rev.* **2021**, *50*, 243.
[8] R. P. Hausinger, *Crit. Rev. Biochem. Mol. Biol.* **2004**, *39*, 21 – 68.
[9] E. G. Kovaleva, J. D. Lipscomb, *Nat. Chem. Biol.* **2008**, *4*, 186 – 193.
[10] M. Sono, M. P. Roach, E. D. Coulter, J. H. Dawson, *Chem. Rev.* **1996**, *96*, 2841 – 2888.
[11] J. Rittle, M. T. Green, *Science* **2010**, *330*, 933 – 937.
[12] S. Shaik, H. Hirao, D. Kumar, *Nat. Prod. Rep.* **2007**, *24*, 533 – 552.
[13] T. G. Traylor, F. Xu, *J. Am. Chem. Soc.* **1988**, *110*, 1953 – 1958.
[14] M. R. Bukowski, P. Comba, A. Lienke, C. Limberg, C. Lopez de Laorden, R. Mas-Ballesté, M. Merz, L. Que, Jr., *Angew. Chem. Int. Ed.* **2006**, *45*, 3446 – 3449; *Angew. Chem.* **2006**, *118*, 3524 – 3528.
[15] P. Barman, A. K. Vardhaman, B. Martin, S. J. Wörner, C. V. Sastri, P. Comba, *Angew. Chem. Int. Ed.* **2015**, *54*, 2095 – 2099; *Angew. Chem.* **2015**, *127*, 2123 – 2127.
[16] O. Cussó, X. Ribas, J. Lloret-Fillol, M. Costas, *Angew. Chem. Int. Ed.* **2015**, *54*, 2729; *Angew. Chem.* **2015**, *127*, 2767.
[17] H. Park, H. M. Ahn, H. Y. Jeong, C. Kim, D. Lee, *Chem. Eur. J.* **2018**, *24*, 8632.

[18] R. V. Ottenbacher, D. G. Samsonenko, E. P. Talsi, K. P. Bryliakov, *ACS Catal.* **2014**, *4*, 1599.
[19] D. Sheet, T. K. Paine, *Chem. Sci.* **2016**, *7*, 5322.
[20] O. Cussó, X. Ribas, M. Costas, *Chem. Commun.* **2015**, *51*, 14285.
[21] G. Olivo, O. Cussó, M. Costas, *Chem. Asian J.* **2016**, *11*, 3148.
[22] W. Wang, Q. Sun, D. Xu, C. Xia, W. Sun, *ChemCatChem* **2017**, *9*, 420.
[23] M. Wu, C.-X. Miao, S. Wang, X. Hu, C. Xia, F. E. Kühn, W. Sun, *Adv. Synth. Catal.* **2011**, *353*, 3014.
[24] O. Cussó, I. Garcia-Bosch, X. Ribas, J. Lloret-Fillol, M. Costas, *J. Am. Chem. Soc.* **2013**, *135*, 14871.
[25] A. Bassan, M. R. A. Blomberg, P. E. M. Siegbahn, L. Que, Jr., *Angew. Chem. Int. Ed.* **2005**, *44*, 2939 – 2941; *Angew. Chem.* **2005**, *117*, 2999 – 3001.
[26] K. Chen, J. Q. Lawrence, *Angew. Chem. Int. Ed.* **1999**, *38*, 2227 – 2229; *Angew. Chem.* **1999**, *111*, 2365 – 2368.
[27] M. Costas, A. K. Tipton, K. Chen, D.-H. Jo, L. Que, *J. Am. Chem. Soc.* **2001**, *123*, 6722 – 6723.
[28] R. Mas-Ballesté, M. Costas, T. van den Berg, L. Que, Jr., *Chem. Eur. J.* **2006**, *12*, 7489 – 7500.
[29] R. Mas-Ballesté, L. Que, *J. Am. Chem. Soc.* **2007**, *129*, 15964 – 15972.
[30] P. D. Oldenburg, Y. Feng, I. Pryjomska-Ray, D. Ness, L. Que, *J. Am. Chem. Soc.* **2010**, *132*, 17713 – 17723.
[31] K. Suzuki, P. D. Oldenburg, L. Que, Jr., *Angew. Chem. Int. Ed.* **2008**, *47*, 1887 – 1889; *Angew. Chem.* **2008**, *120*, 1913 – 1915.
[32] A. M. Zima, O. Y. Lyakin, R. V. Ottenbacher, K. P. Bryliakov, E. P. Talsi, *ACS Catal.* **2017**, *7*, 60 – 69.
[33] W. Nam, R. Ho, J. S. Valentine, *J. Am. Chem. Soc.* **1991**, *113*, 7052 – 7054.
[34] X. Engelmann, D. D. Malik, T. Corona, K. Warm, E. R. Farquhar, M. Swart, W. Nam, K. Ray, *Angew. Chem. Int. Ed.* **2019**, *58*, 4012 – 4016; *Angew. Chem.* **2019**, *131*, 4052 – 4056.
[35] O. Y. Lyakin, R. V. Ottenbacher, K. P. Bryliakov, E. P. Talsi, *ACS Catal.* **2012**, *2*, 1196 – 1202.
[36] R. V. Ottenbacher, D. G. Samsonenko, E. P. Talsi, K. P. Bryliakov, *ACS Catal.* **2016**, *6*, 979 – 988.
[37] O. Cussó, I. Garcia-Bosch, D. Font, X. Ribas, J. Lloret-Fillol, M. Costas, *Org. Lett.* **2013**, *15*, 6158 – 6161.
[38] R. A. Baglia, C. M. Krest, T. Yang, P. Leeladee, D. P. Goldberg, *Inorg. Chem.* **2016**, *55*, 10800 – 10809.
[39] J. Du, C. Miao, C. Xia, Y.-M. Lee, W. Nam, W. Sun, *ACS Catal.* **2018**, *8*, 4528 – 4538.
[40] K. P. Bryliakov, *Chem. Rev.* **2017**, *117*, 11406 – 11459.
[41] E. P. Talsi, K. P. Bryliakov, *Coord. Chem. Rev.* **2012**, *256*, 1418 – 1434.
[42] K. P. Bryliakov, E. P. Talsi, *Coord. Chem. Rev.* **2014**, *276*, 73 – 96.
[43] B. Qiu, D. Xu, Q. Sun, C. Miao, Y.-M. Lee, X.-X. Li, W. Nam, W. Sun, *ACS Catal.* **2018**, *8*, 2479 – 2487.
[44] D. Shen, B. Qiu, D. Xu, C. Miao, C. Xia, W. Sun, *Org. Lett.* **2016**, *18*, 372 – 375.
[45] M. Wu, B. Wang, S. Wang, C. Xia, W. Sun, *Org. Lett.* **2009**, *11*, 3622 – 3625.
[46] J. Park, Y.-M. Lee, K. Ohkubo, W. Nam, S. Fukuzumi, *Inorg. Chem.* **2015**, *54*, 5806 – 5812.
[47] S. Rana, J. P. Biswas, A. Sen, M. Clémancey, G. Blondin, J.-M. Latour, G. Rajaraman, D. Maiti, *Chem. Sci.* **2018**, *9*, 7843 – 7858.
[48] W. Rasheed, A. Draksharapu, S. Banerjee, V. G. Young, Jr., R. Fan, Y. Guo, M. Ozerov, J. Nehrkorn, J. Krzystek, J. Telser, et al., *Angew. Chem. Int. Ed.* **2018**, *57*, 9387 – 9391; *Angew. Chem.* **2018**, *130*, 9531 – 9535.
[49] a) D. Macikenas, E. Skrzypczak-Jankun, J. D. Protasiewicz, *J. Am. Chem. Soc.* **1999**, *121*, 7164 – 7165; b) Also the minimal acid impuritiy present in idomesitylene diacetate might have role in enhancing the epoxidation product formation.
[50] S. Rana, A. Dey, D. Maiti, *Chem. Commun.* **2015**, *51*, 14469 – 14472.
[51] M. Ghosh, K. K. Singh, C. Panda, A. Weitz, M. P. Hendrich, T. J. Collins, B. B. Dhar, S. Sen Gupta, *J. Am. Chem. Soc.* **2014**, *136*, 9524 – 9527.
[52] K. K. Singh, M. K. Tiwari, B. B. Dhar, K. Vanka, S. Sen Gupta, *Inorg. Chem.* **2015**, *54*, 6112 – 6121.
[53] S. Jana, M. Ghosh, M. Ambule, S. Sen Gupta, *Org. Lett.* **2017**, *19*, 746 – 749.
[54] G. Olivo, O. Lanzalunga, S. Di Stefano, *Adv. Synth. Catal.* **2016**, *358*, 843 – 863.
[55] R. D. Arasasingham, G. X. He, T. C. Bruice, *J. Am. Chem. Soc.* **1993**, *115*, 7985 – 7991.
[56] J. M. Garrison, D. Ostovic, T. C. Bruice, *J. Am. Chem. Soc.* **1989**, *111*, 4960 – 4966.
[57] G. Coin, R. Patra, S. Rana, J. P. Biswas, P. Dubourdeaux, M. Clémancey, S. P. de Visser, D. Maiti, P. Maldivi, J.-M. Latour, *ACS Catal.* **2020**, *10*, 10010 – 10020.
[58] T. G. Traylor, A. R. Miksztal, *J. Am. Chem. Soc.* **1989**, *111*, 7443 – 7448.
[59] E. G. Samsel, K. Srinivasan, J. K. Kochi, *J. Am. Chem. Soc.* **1985**, *107*, 7606 – 7617.
[60] Y. Naruta, F. Tani, N. Ishihara, K. Maruyama, *J. Am. Chem. Soc.* **1991**, *113*, 6865 – 6872.
[61] D. Ostovic, T. C. Bruice, *Acc. Chem. Res.* **1992**, *25*, 314 – 320.
[62] C.-M. Che, C.-K. Li, W.-T. Tang, W.-Y. Yu, *J. Chem. Soc. Dalton Trans.* **1992**, 3153 – 3158.
[63] S. N. Dhuri, K.-B. Cho, Y.-M. Lee, S. Y. Shin, J. H. Kim, D. Mandal, S. Shaik, W. Nam, *J. Am. Chem. Soc.* **2015**, *137*, 8623 – 8632.
[64] J. T. Groves, Y. Watanabe, *J. Am. Chem. Soc.* **1986**, *108*, 507 – 508.
[65] B. Wang, Y.-M. Lee, M. Clémancey, M. S. Seo, R. Sarangi, J.-M. Latour, W. Nam, *J. Am. Chem. Soc.* **2016**, *138*, 2426 – 2436.
[66] A. D. N. Vaz, D. F. McGinnity, M. J. Coon, *Proc. Natl. Acad. Sci. USA* **1998**, *95*, 3555 – 3560.
[67] M. Yonemitsu, Y. Tanaka, M. Iwamoto, *J. Catal.* **1998**, *178*, 207 – 213.
[68] M. Ansari, N. Vyas, A. Ansari, G. Rajaraman, *Dalton Trans.* **2015**, *44*, 15232 – 15243.
[69] A. Ansari, A. Kaushik, G. Rajaraman, *J. Am. Chem. Soc.* **2013**, *135*, 4235 – 4249.
[70] A. Ansari, M. Ansari, A. Singha, G. Rajaraman, *Chem. Eur. J.* **2017**, *23*, 10110 – 10125.
[71] S. Shaik, H. Hirao, D. Kumar, *Acc. Chem. Res.* **2007**, *40*, 532 – 542.
[72] T. A. Jackson, J.-U. Rohde, M. S. Seo, C. V. Sastri, R. DeHont, A. Stubna, T. Ohta, T. Kitagawa, E. Münck, W. Nam, et al., *J. Am. Chem. Soc.* **2008**, *130*, 12394 – 12407.
[73] J.-U. Rohde, S. Torelli, X. Shan, M. H. Lim, E. J. Klinker, J. Kaizer, K. Chen, W. Nam, L. Que, *J. Am. Chem. Soc.* **2004**, *126*, 16750 – 16761.
[74] G. Mukherjee, A. Alili, P. Barman, D. Kumar, C. V. Sastri, S. P. de Visser, *Chem. Eur. J.* **2019**, *25*, 5086 – 5098.
[75] M. Ansari, D. Senthilnathan, G. Rajaraman, *Chem. Sci.* **2020**, *11*, 10669 – 10687.
[76] R. Kumar, B. Pandey, A. Sen, M. Ansari, S. Sharma, G. Rajaraman, *Coord. Chem. Rev.* **2020**, *419*, 213397.
[77] M. Puri, L. Que, *Acc. Chem. Res.* **2015**, *48*, 2443 – 2452.
[78] D. Schröder, S. Shaik, H. Schwarz, *Acc. Chem. Res.* **2000**, *33*, 139 – 145.
[79] F. Wang, W. Sun, C. Xia, Y. Wang, *J. Biol. Inorg. Chem.* **2017**, *22*, 987 – 998.
[80] S. Shaik, D. Danovich, A. Fiedler, D. Schröder, H. Schwarz, *Helv. Chim. Acta* **1995**, *78*, 1393 – 1407.
[81] F. P. Guengerich, T. L. Macdonald, *Acc. Chem. Res.* **1984**, *17*, 9 – 16.

[82] J. Bautz, P. Comba, C. Lopez de Laorden, M. Menzel, G. Rajaraman, *Angew. Chem. Int. Ed.* **2007**, *46*, 8067 – 8070; *Angew. Chem.* **2007**, *119*, 8213 – 8216.
[83] J. N. Harvey, M. Aschi, *Faraday Discuss.* **2003**, *124*, 129 – 143.
[84] D. Danovich, S. Shaik, *J. Am. Chem. Soc.* **1997**, *119*, 1773 – 1786.
[85] P. Comba, G. Rajaraman, *Inorg. Chem.* **2008**, *47*, 78 – 93.
[86] M. A. Sainna, S. Kumar, D. Kumar, S. Fornarini, M. E. Crestoni, S. P. de Visser, *Chem. Sci.* **2015**, *6*, 1516 – 1529.
[87] D. Kumar, R. Latifi, S. Kumar, E. V. Rybak-Akimova, M. A. Sainna, S. P. de Visser, *Inorg. Chem.* **2013**, *52*, 7968 – 7979.
[88] S. Shaik, H. Chen, D. Janardanan, *Nat. Chem.* **2011**, *3*, 19 – 27.
[89] D. Lakk-Bogáth, G. Speier, J. Kaizer, *Inorg. Chem. Commun.* **2019**, *107*, 107446.
[90] D. Kumar, H. Hirao, Q. Lawrence, S. Shaik, *J. Am. Chem. Soc.* **2005**, *127*, 8026 – 8027.
[91] L. Bernasconi, E. J. Baerends, *J. Am. Chem. Soc.* **2013**, *135*, 8857.

Manuscript received: February 18, 2021
Accepted manuscript online: April 9, 2021
Version of record online: May 7, 2021

